Journal of King Saud University – Science 34 (2022) 102162

Contents lists available at ScienceDirect

Journal of King Saud University – Science

journal homepage: www.sciencedirect.com

Original article

# Efficient magnetic and antibacterial properties of CdO/ZnO nanocomposites prepared via facile hydrothermal method

C. Uthiram, N. Punithavelan *

*Division of Physics, School of Advanced Sciences, Vellore Institute of Technology (VIT), Chennai Campus, Vandalur-Kelmbakkam Road, Chennai 600 127, India*

ARTICLE INFO

*Article history:*
Received 12 April 2022
Accepted 7 June 2022
Available online 11 June 2022

*Keywords:*
Fuel and capping agent free
Magnetic properties
Antibacterial activity
*Streptococcus pyogenes*
*Klebsiella pneumonia*

ABSTRACT

The effect of molar composition on the efficiency of antibacterial and magnetic properties of binary transition metal oxide nanocomposites synthesized using pH optimized hydrothermal method is reported. Its response to X-ray diffraction confirmed the crystallinity of nanocomposites. The average crystallite size is observed to be 27.37 nm, 30.21 nm and 32.3 nm for 1:1, 2:1 and 1:2 molar ratioed CdO/ZnO nanocomposites respectively. FT-IR spectroscopy revealed the presence of moisture and other functional groups, which is further confirmed the Thermogravimetric analysis showing approximately 1.5% of thermal decomposition within 200 °C in all composition. The synthesized composites are characterized for surface morphology using High-resolution scanning electron microscopy and Energy dispersive X-ray analysis showed mixed nanorods, nanotubes and spheroid structures. The optical band gap of proposed nanocomposites is characterized by UV-diffused reflectance spectroscopy showing the variation of optical band gap confirming the change in a molar proportion of CdO/ZnO nanocomposites particles. Investigation on magnetic properties displayed its paramagnetic behavior by illustrating the hysteresis curves of all nanocomposites. The antibacterial activities of proposed nanocomposites investigated for both Gram-positive and Gram-negative bacteria showed its efficiency towards antibacterial application.


## 1. Introduction

Recently, it has been shown that the deficiency of the mitochondrial transmembrane potentially alters mitochondrial permeability. It is a risky point in two bio microorganisms that often may involve the bioactivity of the samples. Cadmium reduces the level of two micro organisms, consequently motivating the group of the superoxide radicals (Hsu and Kao, 2004). It has been claimed that different dopant concentrations may trigger responses that tend to block the creation of a permeability conversion hole in two bacteria (Zhang et al., 2020). These results indicated the ratio 1:1, 2:1 and 1:2, and their semiconducting dopant with CdO possess notable antimicrobial properties. The ligands' antibacterial activity and their effect have been examined for the two pathogenic bacteria of *Streptococcus pyogenes* and *Klebsiella pneumonia*. The results indicated that their semiconducting oxide materials possess enhanced antimicrobial properties.

The zone of inhibition to enhance biological, antioxidant, antimicrobial, and antibacterial activities is highly elevated for 1:1. One of the main bio mechanisms of cadmium-mediated results is its capacity to improve apoptosis and immune defeat, including the group of allowed radicals specifically in the *Klebsiella pneumonia* mitochondrion (Aghebati-maleki et al., 2014). SEM images showed the rod and a plate-like grain strongly support the proposed mechanism in forming double cationic (Bodade et al., 2008). Dopant with CdO of ZnO will give health care providers a list of all the medicines, herbs, non-prescription drugs, or dietary supplements that may interact with medicine. A few strategies have been answered to integrate ZnO nano sizes, amongst which the fume transportation and affidavit strategy are the maximum generally utilized ones. Not withstanding arrangement stage techniques are engaging owing to the small development temperatures, the capacities for grading up and the capacity of delivering high-thickness clusters (Varghese et al., 2007).

Cadmium oxide (CdO) is an eminent II–VI n-type semiconductor with fascinating properties for optoelectronic applications due to its tremendous bandgap, low electrical resistivity, and high

* Corresponding author.
*E-mail address:* punithavelan.n@vit.ac.in (N. Punithavelan).
Peer review under responsibility of King Saud University.

Production and hosting by Elsevier

https://doi.org/10.1016/j.jksus.2022.102162
1018-3647/

optical transmission in the perceptible space of the solar range. CdO has a stone salt crystal construction with an indirect bandgap of 1.98 eV and a direct bandgap of 2.2 eV to 2.5 eV, making it valuable for an extensive scope of transparent electrodes, solar cells, sensors and photodiodes. As of late, nanostructured CdO has been readied utilizing different procedures, including chemical bath deposition, spray pyrolysis, sol–gel and chemical vapour deposition. Together CdO and ZnO have fascinating properties for optoelectronic applications.

The optical and morphological properties of the nanostructured Cd and Zn oxides blend films have been recently observed (Han et al., 2011). The oxides content proportion can constrain the optical properties and the bandgap of the combination of them together. As of late, heterostructures of ZnO with semiconductor devices or metals have pulled in much consideration due to their upgraded photocatalytic and optical properties (Yousef et al., 2012). The current examination is focused on the blend of CdO/ZnO nanocomposites to research the impact of CdO content on the bandgap of ZnO (Rahman et al., 2017). Various methods concentrated the crystallinity and morphology of the composites. The optical properties were additionally explored and exhibited that the substance of CdO has diminished the bandgap of the nanocomposites (Kumar et al., 2014).

## 2. Experiment

### 2.1. Preparation of CdO/NiO nanocomposites

Cadmium chloride dihydrate ($CdCl_2{\cdot}2H_2O$, 99%), Zinc (II) chloride hexahydrate ($ZnCl_2{\cdot}6H_2O$, 99%) and Sodium hydroxide (NaOH) as precursor materials for the synthesis of CdO/ZnO nanocomposites, suitable quantity of cadmium chloride dihydrate and zinc chloride hexahydrate in a particular proportion was dissolved in distilled water to form a 0.1 M (1:1 ratio) combination of solution. Similarly, we prepared the different ratios like 2:1 and 1:2, respectively. To this mixture, 2 M of NaOH solution was added dropwise with constant stirring. After one hour of stirring, a white precipitate was obtained. The resultant product was transferred into a 100 mL Teflon- lined stainless autoclave, sealed and maintained at 180 °C for 12 h. The product was washed several times with distilled water and acetone and then dried at 100 °C for 1 h in a hot air oven. Finally, the resulting product was calcinated at 500 °C for four hours to obtain the CdO/ZnO nanocomposites.

### 2.2. Growth and maintenance of test microorganism for antimicrobial studies

The test organisms utilized were medical confines *viz., Klebsiella pneumonia* and *Streptococcus pyogenes* obtained from the Department of Microbiology, Bharathiar University, Coimbatore. The bacterial and fungal cultures were sustained on the nutrient agar medium and potato dextrose agar (PDA) medium. The bacterial and fungal cultures were maintained on nutrient broth (NB) at 37 °C, and fungus was sustained on Potato dextrose agar (PDA) at 28 °C. The gram-negative bacteria *Klebsiella pneumonia and* Gram-positive bacteria *Streptococcus pyogenes* were pre-cultured in nutrient broth overnight in a rotary shaker at 37 °C, centrifuged at 10,000 rpm for 5 min, the pellet was suspended in double distilled water, and the cell density was standardized spectro photometrically ($A_{610}$ nm).

### 2.3. Instrumentation

The following estimations described the synthesized nanocomposites: The powder X-ray diffraction (PXRD) was found by utilizing Rigaku (Smart Lab), with CuKα radiation of frequency λ = 1.5406 Å with the diffraction point ranges between 10 and 80 deg. Fourier transformation IR spectroscopic range was recorded between the reaches 400–4000 $cm^{-1}$ using Thermo Scientific Nicolet iS10 infrared spectrophotometer. The optical properties were analyzed utilizing UV-diffuse reflectance spectrometry (Thermo logical – Evolution 300 UV–Vis) between 200–800 nm range. The thermal properties were determined by TG-DTA model SII Nano 7200. The morphological structure was measured using Scanning Electron Microscope (SEM) model FEI QUANTA 200. The magnetic properties were investigated using Vibrating Sample Magnetometer (LAKE SHORE SERIAL NO; 741055387 240 V/50HZ/1.5KVA).

## 3. Result and discussions

### 3.1. Structural analysis

Powder X-ray diffraction technique is used to find out the crystal structure and lattice parameters along with structural modifications and identification of phases of the prepared particles. Fig. 1 shows the X-ray diffraction patterns of CdO/ZnO nanocomposites by the hydrothermal method. The synthesized CdO/ZnO nanocomposite diffraction pattern shows both phases of cubic CdO hexagonal ZnO. The characterization peaks at 2$\theta$ of 31.78°, 33.05°, 34.44°, 36.26°, 38.35°, 47.55°, 55.36°, 56.61°, 62.87°, 66.01°, 67.98°, 96.29° are indexed as the (100), (111), (002), (101), (200), (102), (220), (110), (103), (311), (112) and (222) crystallographic planes, respectively. In this nanocomposite, both the diffraction angles of cubic and hexagonal phases existed for CdO and ZnO (JCPDS card number – 03-065-2908 and 01-089-0510). No contamination peaks were detected, thus representing that the final product was a high purity mixture of CdO and NiO. The crystallite size *(D)* was calculated using Debye Scherrer's Formula (Canbay et al., 2018).

$$D = \frac{0.9\lambda}{\beta \cos\theta} \quad (1)$$

where, $D$ is the crystallite size, $\lambda$ is the X-ray wavelength (0.154 nm), $\beta$ is the full width half maximum intensity (FWHM), and $\theta$ is the bragg's angle (in degrees). Using Eq. (1), the average

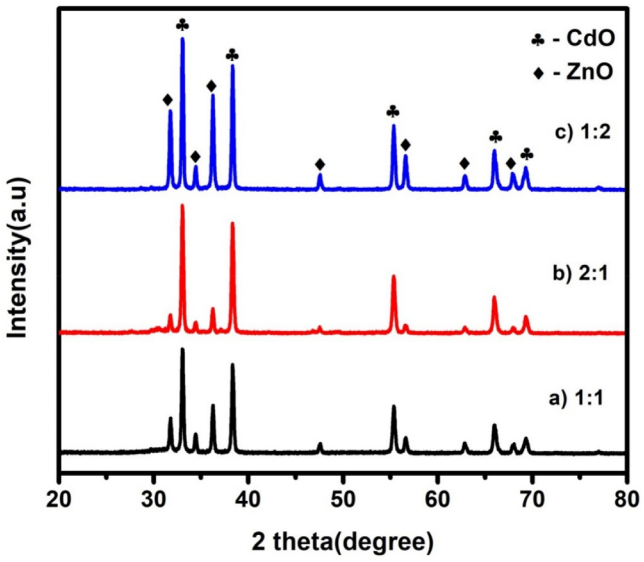


**Fig. 1.** X-ray diffraction peaks of CdO/ZnO nanocomposites for a) 1:1, b) 2:1 and c) 1:2.

crystallite sizes of CdO/ZnO nanocomposites of ratios 1:1, 2:1 and 1:2 were calulcuated as 27.37 nm, 30.21 nm and 32.3 nm.

### 3.2. Bonding analysis

FT-IR spectrum is the characteristic of a precise compound that details its molecular structure, functional groups and intermolecular interfaces. FT-IR spectrum of CdO/ZnO nanocomposite is conveyed in the wavenumber range between 400 and 4000 $cm^{-1}$ and displayed in Fig. 2. The ZnO peak is detected at 511 $cm^{-1}$, which confirms the conversion of $ZnCl_2$ into ZnO (Li et al., 2004; Wahab et al., 2007). The stretching vibration of CdO appears in the range of 708 $cm^1$. The overtone of the CdO/ZnO is observed at 858 $cm^{-1}$, which proposes that the creation of tetrahedral coordination of Cd ($CdO_4$) and Zn ($ZnO_4$) is existing (Fernandes et al., 2009). The establishment of cubic CdO and hexagonal ZnO phases are termed by the peaks at 708 $cm^{-1}$ and 511 $cm^{-1}$ correspondingly. The band at 1451 $cm^{-1}$ agrees to the irregular stretching mode of C = O. The band at 1642 $cm^{-1}$ can be connected with the bending vibrations of $H_2O$ fragments. The peak at 2364 $cm^{-1}$ is possibly attributed to the physisorbed $CO_2$ in the surface of the materials. The detected band at 3250 $cm^{-1}$ matches to the O–H mode of vibration (Hivrekar et al., 2017).

### 3.3. Optical properties

The optical absorption spectra of CdO/ZnO nanocomposite were studied by using UV–visible diffuse reflectance spectroscopy. The optical bandgap of the CdO/ZnO nanocomposite is shown in Figs. 3a, 3b and 3c. The bandgap was calculated from the Kubelka–Munk (K-M) function (Zargar et al., 2019). In Kubelka–Munk function *[F(R)]* is usually applied to modification the diffuse reflectance into absorption coefficient ($\alpha$) is given by the relation and commonly used for investigating the powder materials.

$$\alpha = F(R) = \frac{(1-R)^2}{2R} \tag{2}$$

where *F(R)* is the Kubelka–Munk function, $\alpha$ is the absorption coefficient, and *R* is the reflectance.

Diffuse reflectance spectroscopy plays a crucial part in assessing the optical energy bandgap. The Tauc's relation is used to find out the bandgap ($E_g$) of the samples,

$$F(R)h\upsilon = A(h\upsilon - E_g)^n \tag{3}$$

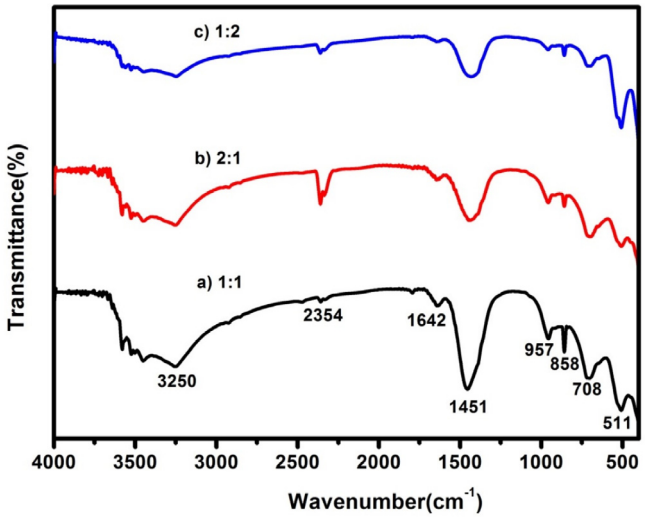


**Fig. 2.** FTIR spectrum of CdO/ZnO nanocomposites for a) 1:1, b) 2:1 and c) 1:2.

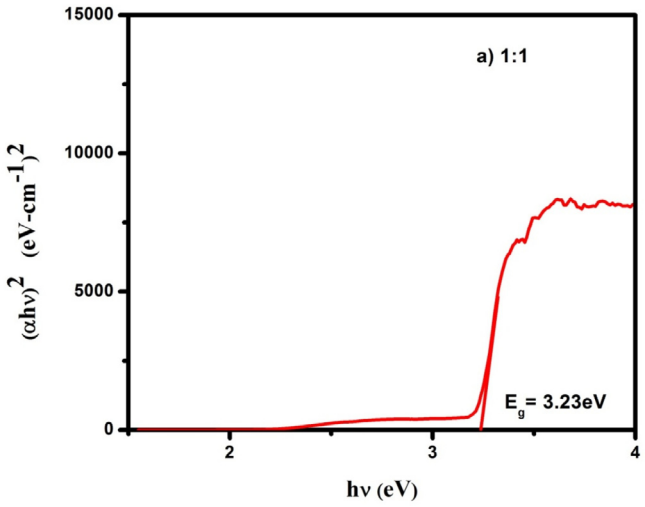


**Fig. 3a.** Optical band gap of CdO/ZnO nanocomposites for 1:1 ratio.

where $n$ = 1/2 for direct allowed transition and $n$ = 2 for indirect allowed transition, $h$ is Planck's constant, $\nu$ is the frequency of light, and $E_g$ is the bandgap energy. The bandgap was calculated between $h\nu$ and $(F(R)h\nu)^2$ in Figs. 3a, 3b and 3c. The extrapolation of the linear section to $(F(R)h\nu)^2 = 0$ provides the band gap value (Yang et al., 2010; Karthik and Dhanuskodi, 2016). The optical band gap value of the CdO/ZnO nanocomposites exhibited the direct bandgap of 3.23 eV for 1:1, 3.24 eV for 2:1 and 3.25 eV for 1:2 ratios, respectively. The optical band gap value increases due to concentration values increased.

### 3.4. TG-DTA analysis

The thermal stability of the synthesized nanocomposite was characterized by using thermogravimetry and differential thermal analysis (TG–DTA). The TG-DTA spectrum of CdO/ZnO nanocomposite is demonstrated in Fig. 4a. The TG–DTA spectrum was confirmed for CdO/ZnO nanocomposite within the temperature scope starting 40 °C to 700 °C through an addition of 10 °C/minute in the argon atmosphere. The initial weight loss (2.09%) obtained the range at 200 °C and can be ascribed to the removal of water molecules from the surface of the nanocomposite. The endothermic pinnacle at 253.57 °C attend with a weight loss of 2.48%, is characteristic of the disappearance of organic residues from the nanocomposites (Mohanraj et al., 2019). In the final step, the weight loss of 1.14% taking place endothermic peak at 297.19 °C is owing to the removal of hydroxyl group and other volatile components (Karthik et al., 2019).

Similarly, the Figs. 4b and 4c shows the different steps of weight losses of CdO/ZnO nanocomposites. Additionally, it appears from the TG pinnacle that the sample can be totally decayed to CdO/ZnO after being annealed at around 400 °C. Afterwards, there is significant no weight loss occurred as the temperature is expanded, it is the sign of the thermal stability of nanocomposite up to 700 °C.

### 3.5. Morphological analysis

The surface morphology of CdO/ZnO nanocomposite was considered utilizing HR-SEM at different amplifications and appeared in Fig. 5(a–c). The morphology consists of nanorods, nanotube, spheroid as well as agglomerated unshaped particles. Henceforth, the HR-SEM demonstrated the development of ZnO nanorods. Fig. 5(b) shows the HR-SEM picture of CdO/ZnO nanocomposites with the nanorods of coupled semiconductors along side some

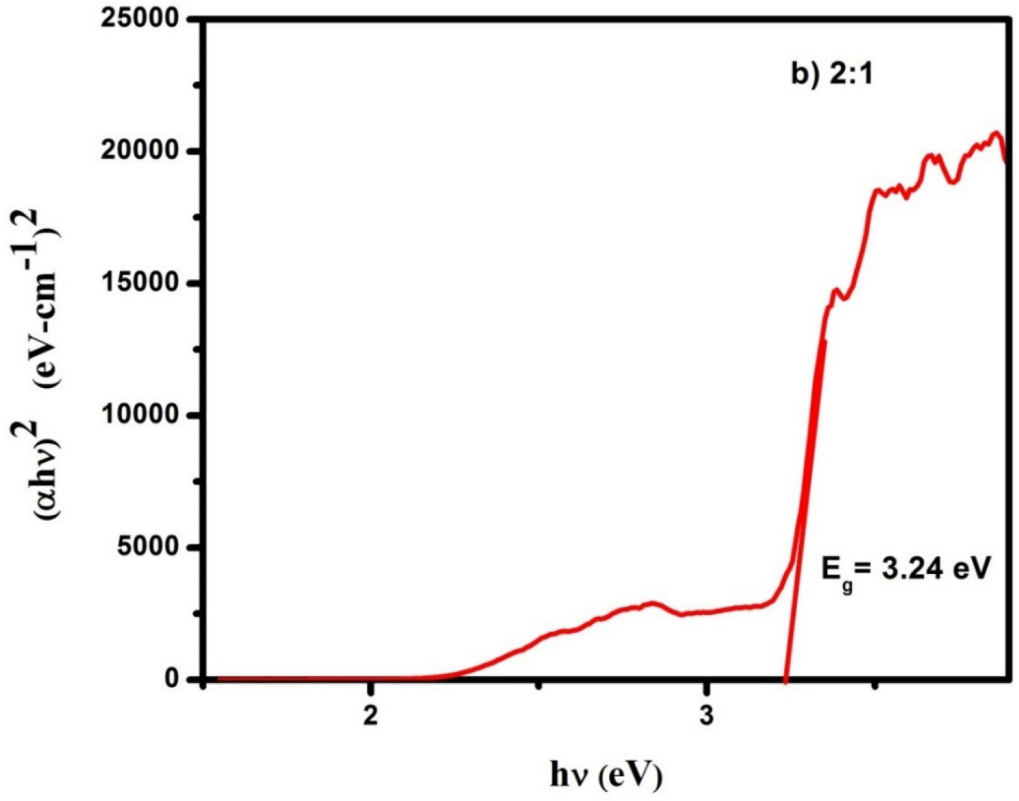


**Fig. 3b.** Optical band gap of CdO/ZnO nanocomposites for 2:1 ratio.

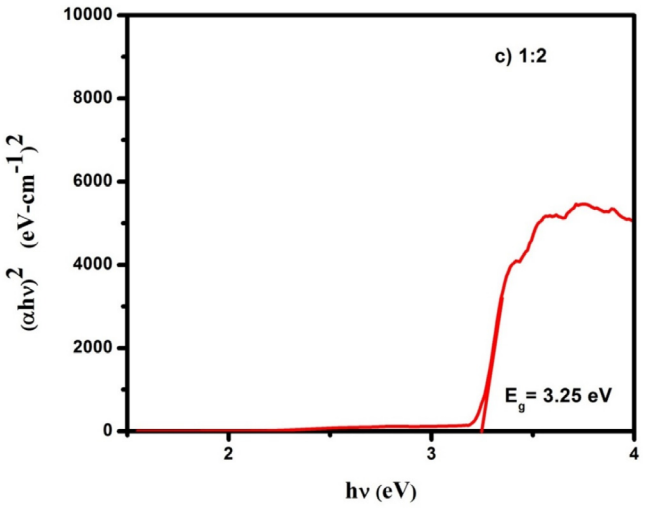


**Fig. 3c.** Optical band gap of CdO/ZnO nanocomposites for 1:2 ratio.

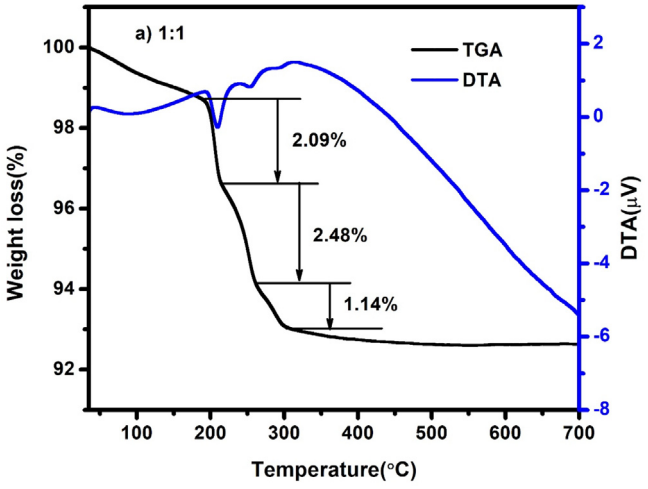


**Fig. 4a.** TG-DTA spectrum of CdO/ZnO nanocomposites for 1:1 ratio.

spherical shape particles. The expansion of contaminations (CdO) over rules the cycle of nucleation also, development, which brings about expanded agglomeration and a change in the morphology of ZnO (Pratheepa and Lawrence, 2019). Morphological SEM analysis gives a hand like structure with high stability crystal nucleation and crystal growth. The appearance of broader diameter and structure grains distribution by SEM analysis can be attributed to the contribution of the short rods and fibres in the following ratios of the samples.

### 3.6. EDX analysis

Fig. 6 shows the EDAX images of the CdO/ZnO nanocomposite. The presence of the components Cd, Zn, and O affirmed composite arrangement, including CdO and ZnO. The atomic percentage composition of Cd, Zn and O were estimated from the EDAX graphical representation with various compositions are shown. These results were well matched with the amount of substance taken as precursor.

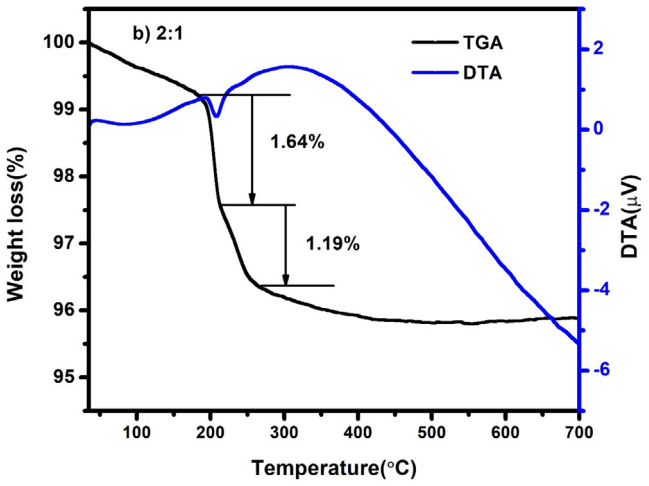


**Fig. 4b.** TG-DTA spectrum of CdO/ZnO nanocomposites 2:1 ratio.

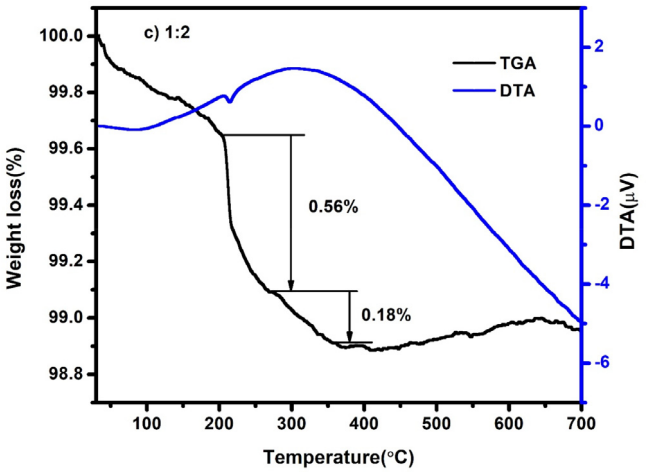


**Fig. 4c.** TG-DTA spectrum of CdO/ZnO nanocomposites 1:2 ratio.

### 3.7. Vibrating Sample Magnetometer study

Fig. 7 demonstrates the room temperature M–H curves of the CdO/ZnO nanocomposites. It tends to be seen that CdO and ZnO nanopowder display paramagnetic behaviour, while the presence of hysteresis loops is noticed for CdO/ZnO nanocomposite was measured and shown in Table 1. In nano dimensions, magnetic commitment can be accomplished through the field-initiated spin of the paramagnetic sublattices. The polarization turn is brought about by the net connection of uncompensated spin with the magnetic field. The paramagnetic requesting saw here for CdO/ZnO nanocomposite may be because of the moderately high anisotropy commitment of $Zn^{2+}$ ions (Karthik et al., 2019). The saturation magnetization (Ms) value of the 2:1 ratio ($992.21 \times 10^{-6}$ emu $g^{-1}$) was established to be less than that of the 1:1 ratio of CdO/ZnO ($1.4062 \times 10^{-3}$ emu $g^{-1}$). The diminished magnetization noticed for the composite may be because of the presence of broken lattice distortion and bonds (Zhang et al., 2020), which may have happened because of the homogeneous combining of the mutually CdO and ZnO. The hysteresis curves of the CdO/ZnO nanocomposite displays delicate magnetic behaviour with coercivity esteems being equivalent to 48.238 Oe, 77.389 Oe and 39.249 Oe respectively (Fig. 8).

### 3.8. Antibacterial activities

In CdO content, when ZnO is doped, the intrinsic band alignment would always act as a dominant factor in antibacterial activity because its adsorption of bacterial strain for the two bacteria was tested and the details were shown in Table 2.

The samples were tested through the good diffusion technique. Different extracts (10, 20, 30 μg/ml) were prepared by reconstructing them with methanol. The test micro-organisms were seeded into a particular medium by spread plate method 10 μl (10 cells/ml) with the 24 h cultures of bacteria growth in nutrient broth. Further, the different concentrations of inhibitions were shown in the Tables 3–5. Later solidifying the filter paper wells (5 mm in diameter) saturated with the extracts were located on test organism-seeded plates. Penicillin (10 μg) is used as a common for the antibacterial test. The antibacterial assay plates were incubated at 37 °C for 24 h. The diameters of the inhibition regions were measured in mm. It is found that when the concentration of samples in μl increases zone of inhibition (ZOI) also increases. So, it is revealed that this sample makes the direct proportion with ZOI and is trying to reach the standard activity in the present work. Perhaps, it makes the inverse proportion with ZOI for the higher molar concentration (Somasundaram and Rajan, 2018).

### 3.9. Proposed mechanism of antibacterial activity

By using the well diffusion method, the antibacterial activities were investigated for both Gram positive and Gram negative bacteria namely *Streptococcus pyogenes* and *Klebsiella pneumonia*. The basic surface morphology of these microbes is gorged pearl beads and capsules, respectively, which means basic structure and its well-constructed bio walls.

Generally, the antibacterial action in utilizing metal oxide nanoparticles can be carried out by the formation of five entities such as metal ions, hydroxyl ions $OH^-$, hydrogen peroxide $H_2O_2$, negative oxygen ions $O^-$ and Reactive oxygen species (ROS). The generation of these kind free species from the metal oxide sample can be initiated by injecting the photon energy on it during the active period of interaction between the bacteria and NPs. This activity depicted as described image explained the antibacterial mechanism as shown in the Fig. 9 were inferring the releasing of hydrogen peroxide and negative ions under the influence of electromagnetic wave in the visible region. So this fig depicted the effective ROS generation under the external visible light (Al-Hada et al., 2017). Usually, the ability of antibacterial action of double cationic samples depends upon four main parameters such as (i) population of ROS (ii) morphology of the NPs (iii) concentration of cationic releases (iv) concentration of negative ions releases. In the present work, a double cationic nanopowder which includes both $Cd^{2+}$ and $Zn^{2+}$ synthesized are express the more superior action than single cationic samples. From the crystallographic, optical and EDAX data, it is revealing that concentration of $Zn^{2+}$ and $Cd^{2+}$ ions are generated from these double cationic samples effectively. The production of $H_2O_2$, $OH^-$, $Zn^{2+}$, $Cd^{2+}$ and ROS depends upon the electromagnetic interaction of external photons which initiate the splitting of molecules as this species due to the basic phenomenon of formation of singly ionized oxygen vacancies and both metal oxide's interstitial in the samples. Notably, the rod and plates like morphologies act as the driller as well as sticker agents to perturb and penetrate the thick cell walls of both gram positive and negative bacteria. Due to this action, more deformation and dissociation were occurring in the cell finally makes more pores are formed. These pores are act as the entrance for the ROS and other ionic species which will be penetrated the parts of the cell simultaneously (Anitha et al., 2018).

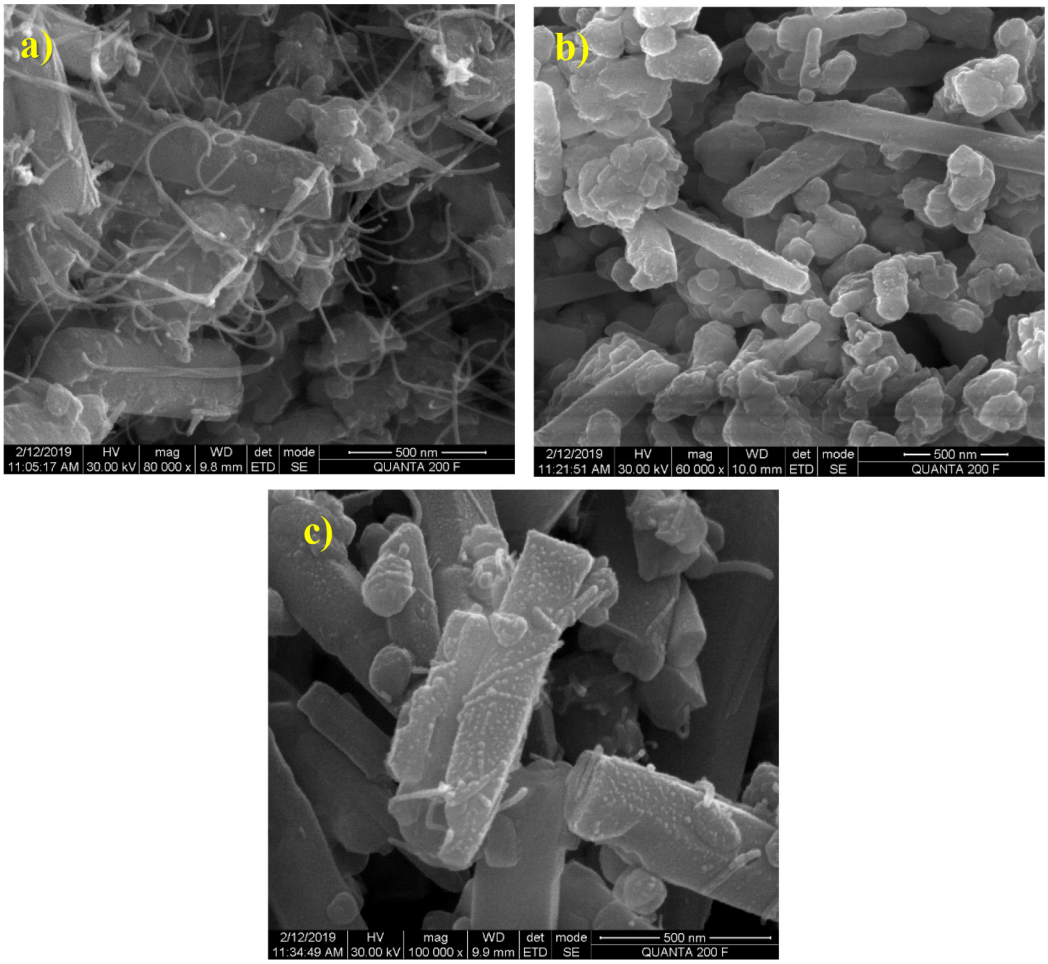


**Fig. 5.** HR-SEM images of CdO/ZnO nanocomposites for a) 1:1, b) 2:1 and c) 1:2.

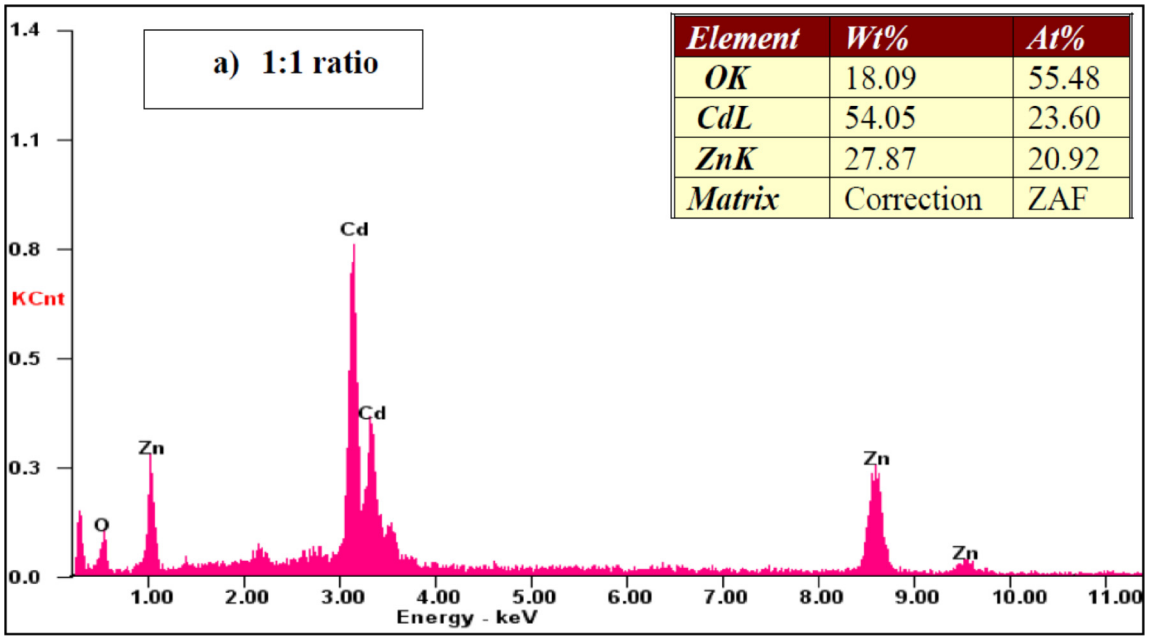


**Fig. 6a.** EDX spectra of the CdO/ZnO nanocomposites for 1:1 ratio.

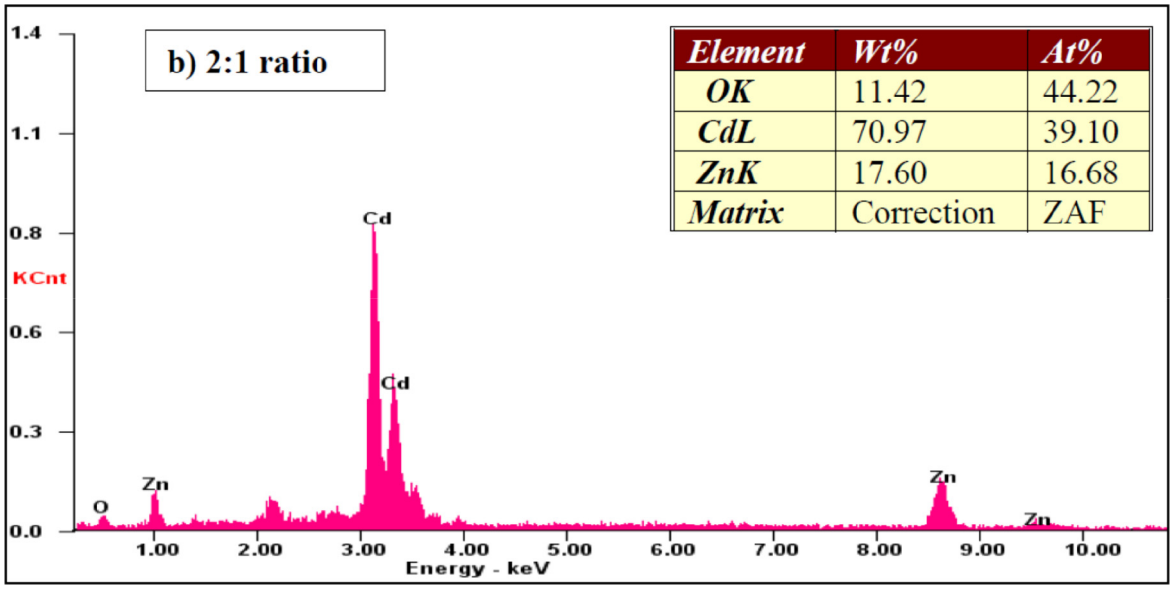


**Fig. 6b.** EDX spectra of the CdO/ZnO nanocomposites for 2:1 ratio.

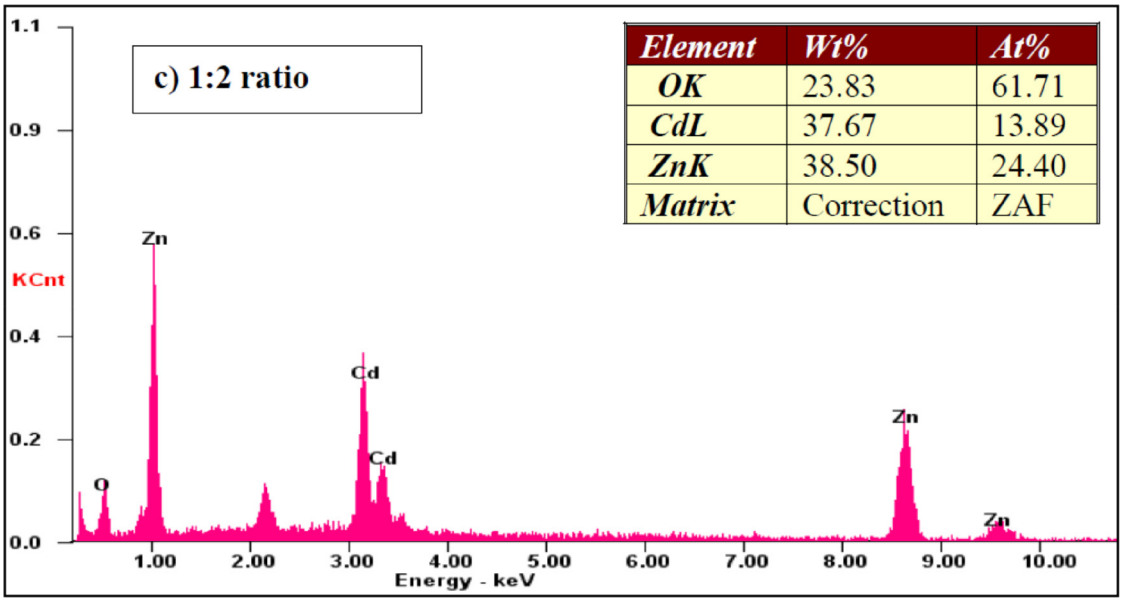


**Fig. 6c.** EDX spectra of the CdO/ZnO nanocomposites for 1:2 ratio.

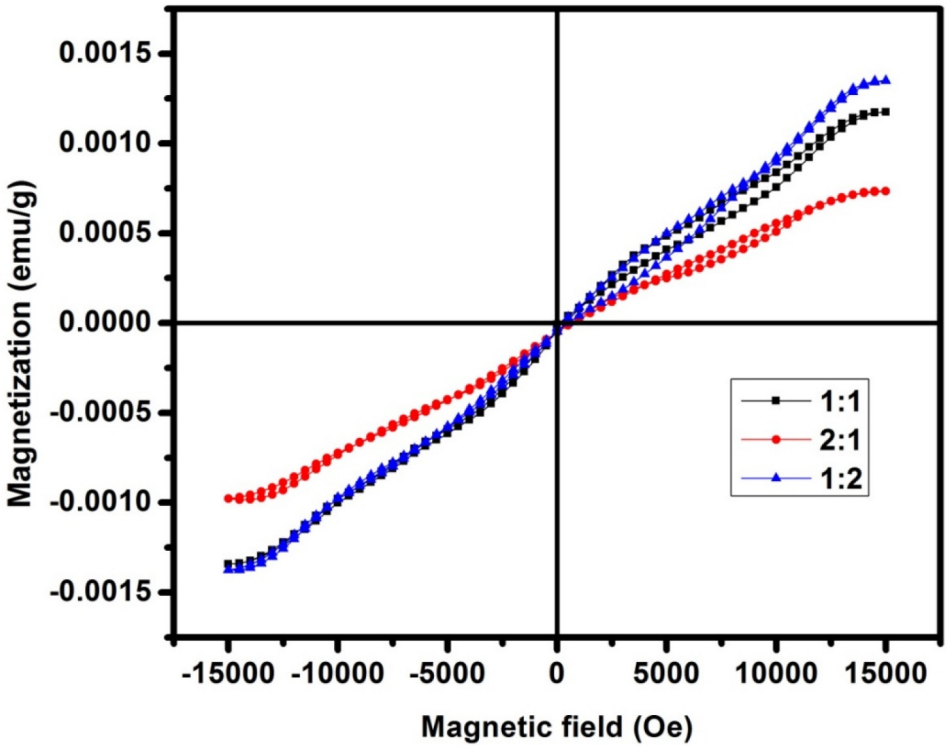


**Fig. 7.** VSM curves of CdO/ZnO nanocomposites for a) 1:1, b) 2:1 and c) 1:2.

**Table 1**
Calculated magnetic properties of CdO/ZnO nanocomposites.

| Sample code | Temperature(°C) | Magnetic saturation(Ms) (emu $g^{-1}$) | Magnetic retentivity(Mr) (emu $g^{-1}$) | Coercivity (Hc) (Oe) |
|---|---|---|---|---|
| 1:1 | 500 | $1.4062 \times 10^{-3}$ | $8.9661 \times 10^{-6}$ | 49.238 |
| 2:1 | 500 | $992.21 \times 10^{-6}$ | $11.090 \times 10^{-6}$ | 77.389 |
| 1:2 | 500 | $1.5097 \times 10^{-3}$ | $7.2029 \times 10^{-6}$ | 39.249 |

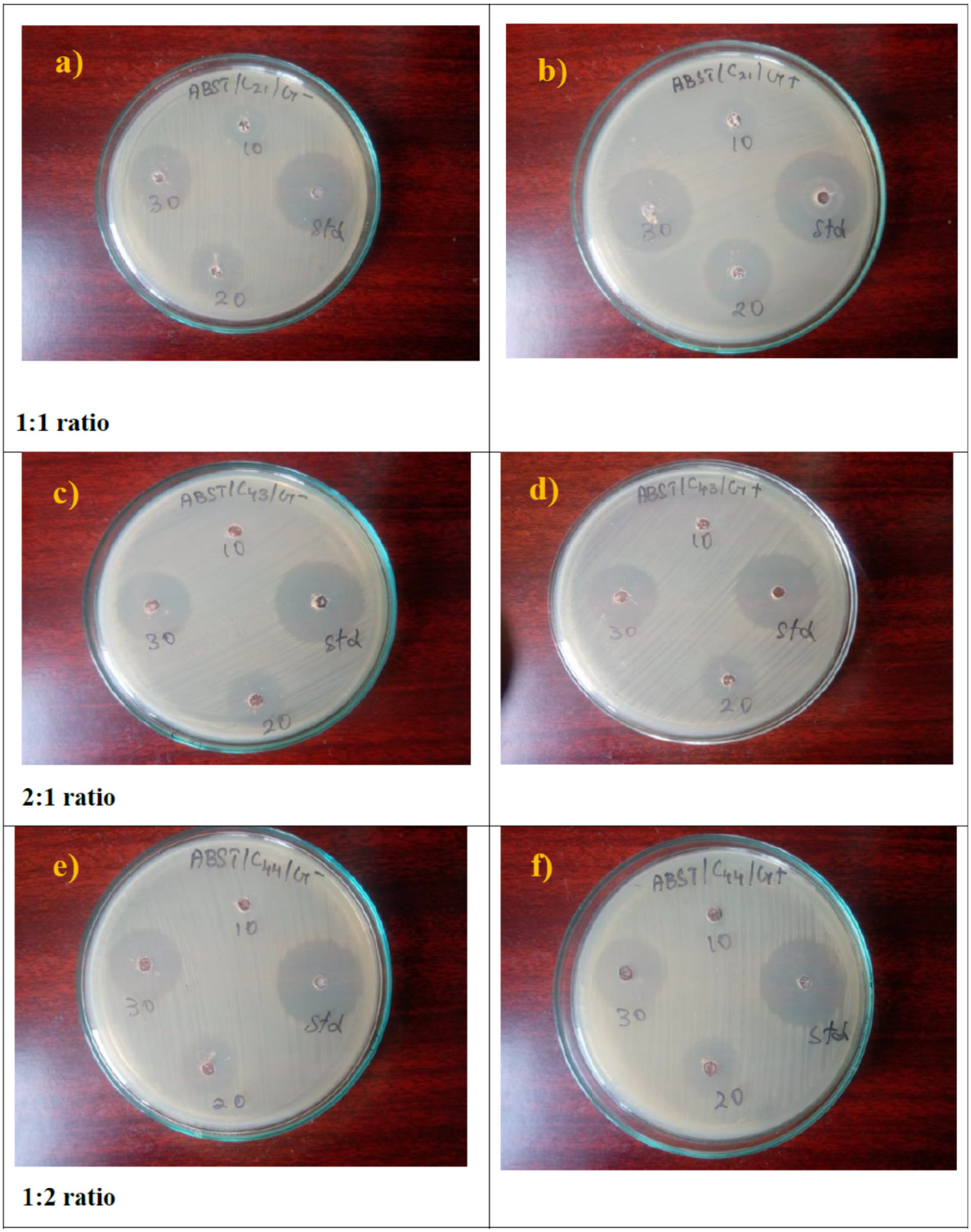


**Fig. 8.** Antibacterial activities of CdO/ZnO nanocomposites (a-b) 1:1 ratio (c-d) 2:1 ratio (e-f) 1:2 ratio.

**Table 2**
Composition of Nutrient agar medium.

| | |
|---|---|
| Peptone | 5.0 g |
| Beef extract | 3.0 g |
| Agar | 15.0 g |
| Distilled water | 1000 mL |
| pH | 7.0 |

## 4. Conclusion

Cost-effective soft chemical approached hydrothermal synthesis technique is a successful method in forming the metal oxide nanocomposites (CdO/ZnO NCs)). The PXRD analysis confirmed that the synthesized NCs belongs to hexagonal wurtzite heterostructure. From the HR-SEM surface morphologies, the mixture of different nano dimensions was found to exhibit nanor-

**Table 3**
The antibacterial activity of CdO/ZnO nanocomposites under zone inhibition method for 1:1 ratio.

| S.No | Pathogenic bacteria | Zone of inhibition (mm) | | | Standard (Penicillin) |
|---|---|---|---|---|---|
| | | 10 µl | 20 µl | 30 µl | |
| 1. | *Streptococcus pyogenes* | 03 | 06 | 08 | 10 |
| 2. | *Klebsiella pneumonia* | 03 | 06 | 07 | 09 |

**Table 4**
The antibacterial activity of CdO/ZnO nanocomposites under zone inhibition method for 2:1 ratio.

| S.No | Pathogenic bacteria | Zone of inhibition (mm) | | | Standard (Penicillin) |
|---|---|---|---|---|---|
| | | 10 µl | 20 µl | 30 µl | |
| 1. | *Streptococcus pyogenes* | 00 | 03 | 06 | 10 |
| 2. | *Klebsiella pneumonia* | 00 | 04 | 07 | 10 |

**Table 5**
The antibacterial activity of CdO/ZnO nanocomposites under zone inhibition method for 1:2 ratio.

| S.No | Pathogenic bacteria | Zone of inhibition (mm) | | | Standard (Penicillin) |
|---|---|---|---|---|---|
| | | 10 µl | 20 µl | 30 µl | |
| 1. | *Streptococcus pyogenes* | 00 | 03 | 06 | 09 |
| 2. | *Klebsiella pneumonia* | 00 | 03 | 06 | 10 |

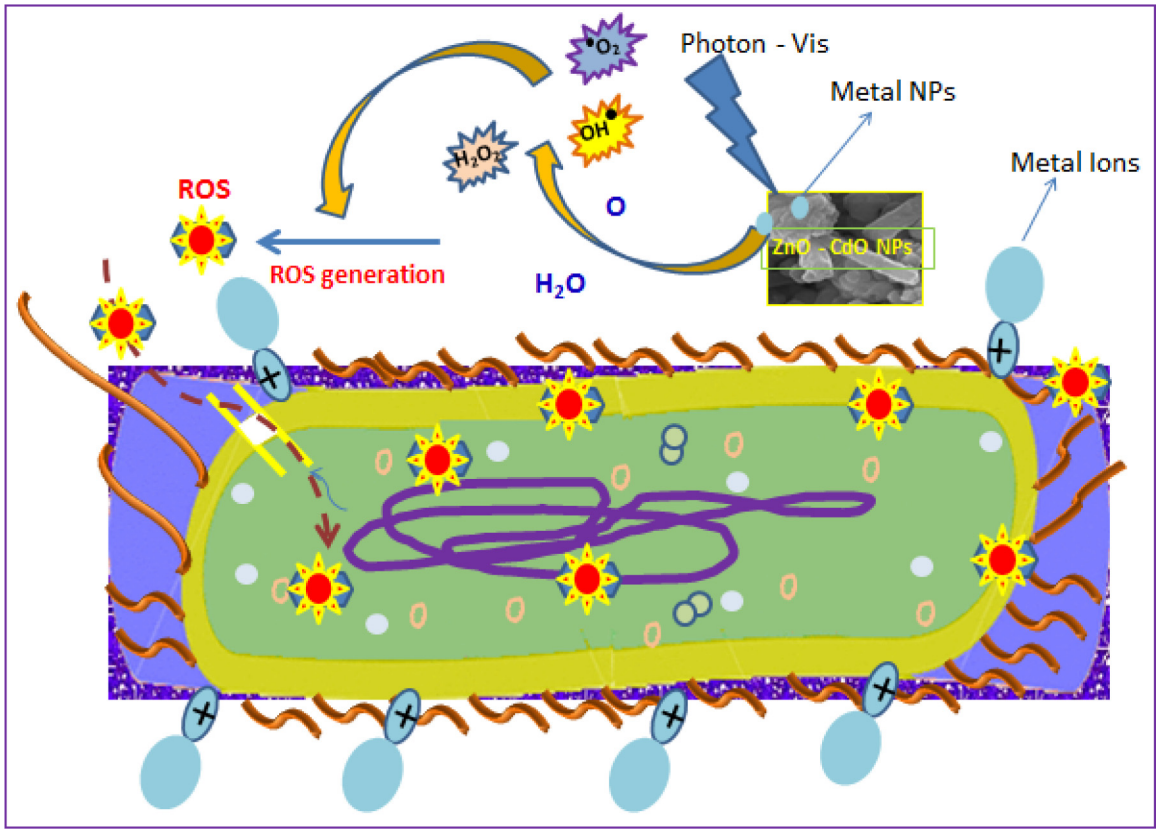


**Fig. 9.** Antibacterial mechanism of CdO/ZnO nanocomposites.

ods, nanotube and unshaped like morphologies. The EDX spectrum data clearly showed elemental compositions with considerable peaks with the expected percentage for three samples. Moreover, the computed FT-IR spectra, the different vibrational functional group frequencies were assigned for the CdO/ZnO NCs. Further from the optical study report, the energy bandgap of ZnO doped CdO NCs were estimated as 3.23, 3.24 and 3.25 eV from the tauc plot. From the antibacterial application experiment, the releasing soldiers such as $H_2O_2$, $OH^-$, $Zn^{2+}$, $Cd^{2+}$ and ROS provide the notable radii of zone of inhibition for different strains which was direct proportion with concentration of entitled NCs samples.

## Declaration of Competing Interest

The authors declare that they have no known competing financial interests or personal relationships that could have appeared to influence the work reported in this paper.

## References


Hsu, Y.T., Kao, C.H., 2004. Cadmium toxicity is reduced by nitric oxide in rice leaves. Plant Growth Regul. 42, 227–238. https://doi.org/10.1023/B:GROW.0000026514.98385.5c.

Zhang, B., Li, B.o., Gao, S., Li, Y., Cao, R., Cheng, J., Li, R., Wang, E., Guo, Y., Zhang, K., Liang, J., Liu, B., 2020. Y-doped TiO2 coating with superior bioactivity and antibacterial property prepared via plasma electrolytic oxidation. Mater. Des. 192, 108758.

Aghebati-maleki, L., Salehi, B., Behfar, R., Saeidmanesh, H., Ahmadian, F., Sarebanhassanabadi, M., et al., 2014. Designing a hydrogen peroxide biosensor using catalase and modified electrode with magnesium oxide nanoparticles. Int. J. Electrochem. Sci. 9, 257–271.

Bodade, A.B., Bende, A.M., Chaudhari, G.N., 2008. Synthesis and characterization of CdO-doped nanocrystalline ZnO:TiO2-based H2S gas sensor. Vacuum 82, 588–593. https://doi.org/10.1016/j.vacuum.2007.08.015.

Varghese, N., Panchakarla, L.S., Hanapi, M., Govindaraj, A., Rao, C.N.R., 2007. Solvothermal synthesis of nanorods of ZnO, N-doped ZnO and CdO. Mater. Res. Bull. 42, 2117–2124. https://doi.org/10.1016/j.materresbull.2007.01.017.

Han, N., Wu, X., Zhang, D., Shen, G., Liu, H., Chen, Y., 2011. CdO activated Sn-doped ZnO for highly sensitive, selective and stable formaldehyde sensor. Sensors Actuators, B Chem 152, 324–329. https://doi.org/10.1016/j.snb.2010.12.029.

Yousef, A., Barakat, N.A.M., Amna, T., Unnithan, A.R., Al-Deyab, S.S., Yong, K.H., 2012. Influence of CdO-doping on the photoluminescence properties of ZnO nanofibers: effective visible light photocatalyst for waste water treatment. J. Lumin. 132, 1668–1677. https://doi.org/10.1016/j.jlumin.2012.02.031.

Rahman, M.M., Alam, M.M., Asiri, A.M., Islam, M.A., 2017. Ethanol sensor development based on ternary-doped metal oxides (CdO/ZnO/$Yb_2O_3$) nanosheets for environmental safety. RSC Adv. 7, 22627–22639. https://doi.org/10.1039/c7ra01852e.

Kumar, P.S., Selvakumar, M., Bhagabati, P., Bharathi, B., Karuthapandian, S., Balakumar, S., 2014. CdO/ZnO nanohybrids: Facile synthesis and morphologically enhanced photocatalytic performance. RSC Adv. 4, 32977–32986. https://doi.org/10.1039/c4ra02502d.

Canbay, C.A., Biro, S.J., Özkul, İ., 2018. The Hydrothermal Synthesis of ZnO-CdO Composite and Physical and Electrical Characterization, 25–37.

Li, H., Wang, J., Liu, H., Yang, C., Xu, H., Li, X., Cui, H., 2004. Sol - Gel preparation of transparent zinc oxide films with highly preferential crystal orientation. Vacuum 77 (1), 57–62.

Wahab, R., Ansari, S.G., Kim, Y.S., Seo, H.K., Shin, H.S., 2007. Room temperature synthesis of needle-shaped ZnO nanorods via sonochemical method. Appl. Surf. Sci. 253, 7622–7626. https://doi.org/10.1016/j.apsusc.2007.03.060.

Fernandes, D.M., Silva, R., Hechenleitner, A.A.W., Radovanovic, E., Melo, M.A.C., Pineda, E.A.G., 2009. Synthesis and characterization of ZnO, CuO and a mixed Zn and Cu oxide. Mater. Chem. Phys. 115, 110–115. https://doi.org/10.1016/j.matchemphys.2008.11.038.

Hivrekar, M.M., Sable, D.B., Solunke, M.B., Jadhav, K.M., 2017. Network structure analysis of modifier CdO doped sodium borate glass using FTIR and Raman spectroscopy. J Non Cryst Solids 474, 58–65. https://doi.org/10.1016/j.jnoncrysol.2017.08.028.

Zargar, R.A., Shah, A.H., Arora, M., Mir, F.A., 2019. Crystallographic, spectroscopic and electrical study of ZnO:CdO nanocomposite-coated films for photovoltaic applications. Arab J Sci Eng 44, 6631–6636. https://doi.org/10.1007/s13369-019-03823-9.

Yang, Z.-X., Zhong, W., Yin, Y.-X., Du, X., Deng, Y.u., Au, C., Du, Y.-W., 2010. Controllable synthesis of single-crystalline CdO and $Cd(OH)_2$ nanowires by a simple hydrothermal approach. Nanoscale Res. Lett. 5 (6), 961–965.

Karthik, K., Dhanuskodi, S., 2016. Structural and optical properties of microwave assisted CdO-NiO nanocomposite. AIP Conf. Proc. 1731. https://doi.org/10.1063/1.4947675.

Mohanraj, K., Balasubramanian, D., Chandrasekaran, J., 2019. Synthesis and characterization of ruthenium-doped CdO nanoparticle and its n-RuCdO/p-Si junction diode application. J. Alloy. Compd. 779, 762–775. https://doi.org/10.1016/j.jallcom.2018.11.264.

Karthik, K., Dhanuskodi, S., Gobinath, C., Prabukumar, S., Sivaramakrishnan, S., 2019. Multifunctional properties of CdO nanostructures Synthesized through microwave assisted hydrothermal method. Mater Res Innov 23, 310–318. https://doi.org/10.1080/14328917.2018.1475443.

Pratheepa, M.I., Lawrence, M., 2019. Synthesis of pure, Cu and Zn doped CdO nanoparticles by co-precipitation method for supercapacitor applications. Vacuum 162, 208–213. https://doi.org/10.1016/j.vacuum.2019.01.042.

Zhang, J., Ding, E., Xu, S., Li, Z., Fakhri, A., Gupta, V.K., 2020. Production of metal oxides nanoparticles based on poly-alanine/chitosan/reduced graphene oxide for photocatalysis degradation, anti-pathogenic bacterial and antioxidant studies. Int. J. Biol. Macromol. 164, 1584–1591. https://doi.org/10.1016/j.ijbiomac.2020.07.291.

Somasundaram, G., Rajan, J., 2018. Effectual Role of Abelmoschus esculentus (Okra) extract on morphology, microbial and photocatalytic activities of CdO tetrahedral clogs. J. Inorg. Organomet. Polym Mater. 28, 152–167. https://doi.org/10.1007/s10904-017-0695-5.

Al-Hada, N.M., Kamari, H.M., Abdullah, C.A.C., Saion, E., Shaari, A.H., Talib, Z.A., et al., 2017. Down-top nanofabrication of binary (CdO)x(ZnO)1−x nanoparticles and their antibacterial activity. Int J Nanomedicine 12, 8309–8323. https://doi.org/10.2147/IJN.S150405.

Anitha, S., Suganya, M., Prabha, D., Srivind, J., Balamurugan, S., Balu, A.R., 2018. Synthesis and characterization of NiO-CdO composite materials towards photoconductive and antibacterial applications. Mater. Chem. Phys. 211, 88–96. https://doi.org/10.1016/j.matchemphys.2018.01.048.